Characterization of the Metal−Ceramic Bonding in the Ag/MgO(001) Interface from ab Initio Calculations

Björn Herschend,[†] Kersti Hermansson,*[,†] Maria Alfredsson,[†] Yuri F. Zhukovskii,[‡] Eugene A. Kotomin,[‡] and Patrick W. M. Jacobs[§]

Department of Materials Chemistry, The Ångström Laboratory, Uppsala University, Box 538, S-751 21 Uppsala, Sweden, Institute of Solid State Physics, University of Latvia, 8 Kengaraga, Riga LV-1063, Latvia, and Department of Chemistry, University of Western Ontario, N6A 5B7 London, Canada

Received: March 5, 2003; In Final Form: June 18, 2003

The nature of the metal−ceramic interaction in the Ag/MgO(001) interface is studied using periodic Hartree−Fock calculations with density functional theory a posteriori correlation corrections. Different aspects of the Ag−MgO interaction have been studied by analysis of the electronic properties: total and projected density of states, multipole moments, bond population, and the difference electron density. By linking these properties to the adsorption energy and making a comparative analysis for interfaces with different degrees of coverage and different adsorption models (one- and two-sided adsorption), a detailed description of the Ag−MgO has been acquired.

1. Introduction

Metal oxide and other ceramic surfaces covered by thin metal films play an important role in many fields of modern technology, including metal−matrix composites in various microelectronic uses, recording media, catalysis, etc.[1−4] One of the most technologically widespread ceramic materials is MgO (magnesia). Various metal/MgO(001) interfaces have been studied in the 1990s, both experimentally[5−11] and theoretically.[12−32] An understanding of the geometric and electronic structure in the interfacial region between the metal and the oxide at an atomic scale is vital to ensure a continued and controlled improvement of these materials and of their use in different technological devices.

Electronic structure calculations of metal/MgO interfaces have been performed with a variety of methods at various levels of theory. Finite-cluster models of the metal/MgO interfaces were studied using both HF[18] and DFT[20,26] methods. An embedded-cluster method was applied using a DFT approach.[27,31] Periodic slab calculations have mainly used different DFT methods[12−16,19,24,28] based on either the local density approximation (LDA) or the generalized gradient approximations (GGA) using either full-potential methods such as full potential linear muffin-tin orbital (FLMTO) and full-potential linearized augmented-plane-waves (FLAPW) or pseudopotential plane-wave methods (PP-PW). The effects of the exact treatment of exchange in slab calculations of the Ag/MgO(001) interface were recently studied in a series of HF calculations with a posteriori electron correlation corrections (HF-CC).[23,25,30,32] Two simpler atomistic methods, the semiempirical image interaction model (IIM)[17] and classical simulations,[21] have also been applied to Ag/MgO(001) interfaces. IIM simulations[17] combine image interaction calculations between the substrate ions and a free-electron metal (with a Fermi cutoff) with HF calculations of short-range interactions between the metal atoms and ion cores. The classical simulations of Purton et al.[21] contained a few hundred relaxed atoms and exploited different kinds of interatomic potentials.

Despite many differences between the aforementioned calculations, several general conclusions can be drawn. Silver adhesion on the oxide substrates occurs mainly due to interaction between the Ag 4d and O 2p energy bands. The formation of the bond across the interface seems to be caused by a complex charge redistribution in the Ag layer,[23,25] but not very much charge transfer or orbital overlap occur. The interaction between the atoms of a noble transition metal and a defect-free MgO(001) substrate is to be characterized as comparatively weak physisorption rather than chemisorption, with the adsorption energy smaller than 0.5 eV per adsorbed metal atom. Surface defects on the MgO(001) substrate markedly increase the interface bond strength,[27,30] and initial nucleation of 2D metal clusters at low coverage has been suggested to occur just at such defects.[10] However, even on the perfect MgO(001) substrate, the growth of metal films usually gives rise to 3D islands; this was established both experimentally[5,7,8] and theoretically.[32] A layer-by-layer growth for Ag deposited on the vacuum-cleaved MgO(001) substrate has been found to be metastable.[6,9]

In spite of the impressive number of studies presented for Ag/MgO(001) so far, there exists no systematic study of how *the electronic properties* of a Ag/MgO(001) interface varies with the Ag coverage, starting from adsorption of almost isolated metal atoms. In this paper we present such results and try to establish the effects of the metal on the electronic properties of the oxide and vice versa. Such insights have important practical applications. If a ceramic support induces a significant charge redistribution in a deposited metal film, it will surely have a bearing on the catalytic properties of the metal (and vice versa for the oxide). A redistribution of electronic charge may also affect the conductivity in the metal layer itself, with important consequences for microelectronic applications of the metal/metal oxide interface. Thus, in this paper, an analysis of the interfacial

* Corresponding author. Fax: (46) 18513548. E-mail address: kersti@mkem.uu.se.
[†] Uppsala University.
[‡] University of Latvia.
[§] University of Western Ontario.

10.1021/jp030305a CCC: $25.00
Published on Web 10/07/2003

bond-induced changes in the density of states (DOS) projected on O 2p and Ag valence 4d states is presented, as well as the changes in atomic multipole moments and the electronic charge distribution, $\rho(\vec{r})$. The evolution of these properties with increasing Ag coverage is monitored. Moreover, the effect of two-sided metal adsorption compared to one-sided adsorption is investigated.

2. Method

2.1. Level of Calculation and Basis Set. Periodic ab initio calculations using linear combinations of Gaussian-type functions (LC GTF) were performed at the Hartree−Fock level with a posteriori DFT correlation corrections using the CRYSTAL98 code.[33] This method has previously been successfully applied to similar systems,[23,25,29,30] and because the Ag overlayers in this study are very thin, the interfaces studied here should not have a metallic character.[34] Thus, the use of the HF-CC method is justified.

For the interface structure optimization, we have used various a posteriori electron correlation corrections to the total energy, not only the PWGGA correlation functional[35] as earlier,[23] but also both GGA (Lee−Yang−Parr[36]) and LSD (Perdew−Zunger[37] and Vosko−Wilk−Nusair[38]) functionals. Such corrections are important because we will compare our ab initio results with previous theoretical studies, many of which were DFT calculations, based on either LSD or GGA exchange and correlation functionals, as mentioned in the Introduction. In the current paper, the basis sets for the magnesium and oxygen ions were taken from ref 39 and consist of all-electron 8-61G and 8-51G (i.e., s and sp shells) for Mg and O, respectively. The Ag atoms were modeled using a small-core Hay−Wadt effective core potential[40] and a 311-31G basis (sp and 4d shells) for the remaining 19 electrons. This basis set was initially developed for AgCl,[41] but the outer Ag exponents have later been reoptimized.[23,25]

For some of the systems, the SCF calculations did not converge using a standard procedure. For these systems, a level shift procedure[42] with shifts as large as 1 hartree had to be used. The same level shift was introduced in all calculations. Several control calculations were performed for the nonproblematic cases, and it was checked that imposing the large level shift did not have any effect on the final result.

2.2. System Geometry. In this paper, we have modeled periodic slabs with two infinite dimensions (*x*- and *y*-directions) and with finite thickness along the *z*-axis, normal to the perfect MgO(001) surface. The Ag coverage (θ) was varied from a 0.25 submonolayer up to a bilayer (Figure 1). A 2 × 2 supercell was used in all calculations. One-sided adsorption was used together with three- and five-layer MgO slabs and two-sided adsorption with five- and seven-layer slabs. The maximum number of layers of the MgO substrate was larger for the two-sided adsorption model, to allow us to investigate the possible interaction between the upper and lower Ag overlayers. In this case, silver atoms were placed symmetrically on both surfaces of the slab, to maintain the mirror plane in the middle of the slab parallel to the surface. In addition, isolated MgO(001) and Ag(001) slabs, as well as bulk magnesia, have been studied, primarily as reference systems.

The Ag atoms have been positioned above the surface O^{2-} ions only. This has been found to be the most favorable position in both theoretical[12,13,16,18−21,23−26] and experimental studies[5,8−11] of metal adhesion on the MgO(001) substrate. The IIM study by Duffy et al.[17] is an exception; here the position over Mg^{2+} ions was found to be the most favorable site. However, the choice of *image plane* in that study was complicated by the fact that the polarization of the metal overlayer over the Mg^{2+} site is very different from the polarization for adsorption over the O^{2-} site. This is likely the reason for the different results from the IIM calculations.

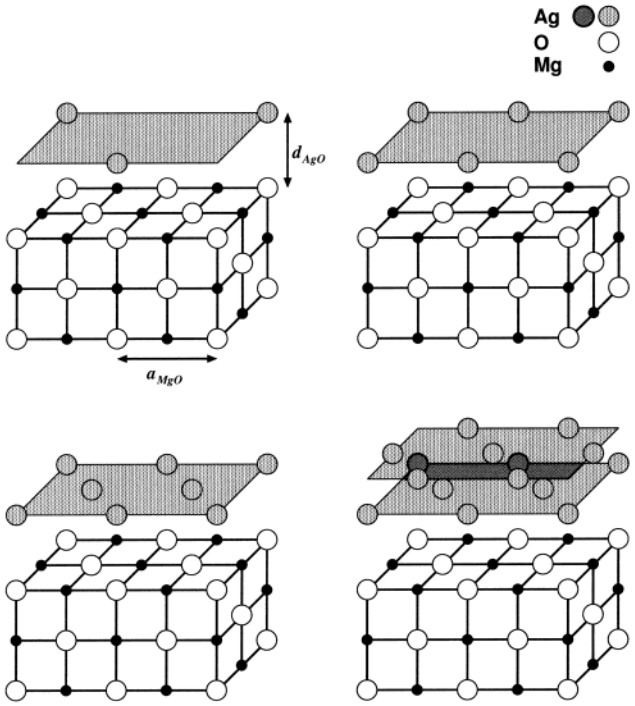

Figure 1. Schematic pictures of 1/4, 1/2, monolayer and bilayer Ag coverage over MgO(001).

Here first the lattice constant for the pure MgO(001) substrate was optimized for a 2 × 2 supercell and was found in the range between 4.06 and 4.15 Å for various correlation functionals and adhesion models, somewhat smaller than the corresponding calculated values for the bulk. The experimental bulk value is 4.205 Å.[39] In the following, for all systems, we have used the optimized *a* value for a five-layer slab with the Perdew−Wang GGA functional: 4.06 Å. The Ag−O^{2-} interface distance was then optimized for all interface systems keeping the rest of the slab geometries fixed. The interplanar Ag−Ag distance in the bilayer was fixed at 2.03 Å.

The adsorption energy per site, $E_{ads/site}$, was calculated according to the equation: $E_{ads/site} = -(E_{Ag/MgO} - E_{isolatedAg} - E_{isolatedMgO})/n_{sites}$, where $E_{Ag/MgO}$ is the energy for the interface system and $E_{isolatedAg}$ and $E_{isolatedMgO}$ are the energies for the isolated Ag overlayer and the isolated MgO substrate, respectively. n_{sites} is the number of adsorption sites in the calculated cell. For comparison, the adsorption energy per surface and supercell, $E_{ads/surf}$, was also calculated according to the equation: $E_{ads/surf} = -(E_{Ag/MgO} - E_{isolatedAg} - E_{isolatedMgO})/n_{surf}$, where $n_{surf} = 1$ or 2 for one- or two-sided adsorption, respectively. The basis set superposition error was not accounted for in our calculations because it has been shown to be small (<0.005 eV) at this computational level.[29]

2.3. Electronic Properties. For all systems, the density of states (DOS) was calculated using the standard routine in the CRYSTAL98 code.[33] Because a local basis of GTFs is used, the DOS can be projected onto a chosen basis function (PDOS), to estimate the contribution of relevant functions to the interface bonding. The DOS and PDOS dependences on substrate coverage and type of model (one-sided and two-sided adhesion) have been investigated. It should be noted that, in the CRYSTAL

TABLE 1: Adsorption Energies per Surface and Slab Unit Cell ($E_{ads/surf}$) and Per Adsorption Site ($E_{ads/site}$) as Well as Interface Distance (d_{Ag-O}) for Different Coverages (θ) and Different Interface Models[a]

θ	$E_{ads/surf}$/eV	$E_{ads/site}$/eV	d_{Ag-O}/Å
One-Sided Adsorption on Three-Layer MgO(001)			
$^1/_4$	0.202	0.202	2.61
$^1/_2$	0.477	0.238	2.59
1	0.675	0.169	2.71
2	1.312	0.328	2.50
One-Sided Adsorption on Five-Layer MgO(001)			
$^1/_4$	0.202	0.202	2.61
$^1/_2$	0.477	0.239	2.61
1	0.681	0.170	2.70
Two-Sided Adsorption on Five-Layer MgO(001)			
$^1/_4$	0.202	0.202	2.61
$^1/_2$	0.478	0.239	2.61
1	0.692	0.173	2.70
2	1.372	0.343	2.52
Two-Sided Adsorption on Seven-Layer MgO(001)			
$^1/_4$	0.203	0.203	2.61
$^1/_2$	0.479	0.240	2.61
1	0.696	0.174	2.68

[a] The HF−CC method with the Perdew−Wang GGA functional[35] and $a_{MgO} = 4.06$ Å were used in all calculations.

code, all Coulomb interactions are calculated explicitly.[43] Thus, the absolute energy is calculated correctly and DOSs for interfaces with different Ag coverages are directly comparable. The atomic charges, e.g., q_{Ag}, were calculated as standard Mulliken charges. In CRYSTAL, projections of atomic dipole moments $D_{Ag}^{(z)}$ are calculated as matrix elements of atomic orbitals (AO) with the operator z (its direction pointing outward from the surface) and characterize a shift of electron density along the surface normal. The same matrix elements in the AO representation with the operator $2z^2 - x^2 - y^2$ form vertical projections of quadrupole moments $Q_{Ag}^{(2z^2-x^2-y^2)}$. The difference electron density, $\Delta\rho(\vec{r})$, was calculated as the total Hartree−Fock electron density for the Ag/MgO(001) interface slab, $\rho(\vec{r})_{Ag/MgO}$, minus a superposition of the densities for isolated Ag and MgO slabs (both with the same geometry as in the total system): $\Delta\rho(\vec{r}) = \rho(\vec{r})_{Ag/MgO} - \rho(\vec{r})_{isolatedAg} - \rho(\vec{r})_{isolatedMgO}$. $\Delta\rho(\vec{r})$ is presented as 2D plots calculated in representative xz-planes.

3. Results and Discussion

3.1. Optimized Geometries and Adsorption Energies.

The 2×2 supercell has four possible O^{2-} adsorption sites on each surface. Not surprisingly, the $Ag-O^{2-}$ interface distance optimization gives an increasing adsorption energy per surface and supercell, $E_{ads/surf}$, with increasing θ (Table 1). However, the adsorption energy per adsorption site, $E_{ads/site}$, does not follow this trend and this is also supported by the equilibrium $Ag-O^{2-}$ interface distances, which do not display a monotonic decrease with increasing θ. Table 1 also shows that $E_{ads/surf}$ is rather insensitive to the substrate thickness and to whether a one- or two-sided adsorption model is used, but it nevertheless increases slightly with increasing substrate thickness and is slightly larger for two-sided compared to one-sided adsorption. The $E_{ads/site}$ value for the monolayer (for all four interface models) is significantly lower than previously found with the HF-CC method (0.20−0.26 eV)[23,25,29,30] and in DFT studies using FLAPW LDA (0.3 eV)[13] and PP-PW LDA (0.33 eV).[14] Our results are more in line with $E_{ads/site}$ values from PP-PW GGA calculations (0.15−0.16 eV).[14,15] The decrease in $E_{ads/site}$ for the monolayer compared to the lower coverages can be explained as an effect of increasing Ag−Ag interaction when the Ag atoms come close to each other. For the less crowded coverages (i.e., when θ is increased from $^1/_4$ to $^1/_2$) this effect is absent. The higher $E_{ads/site}$ values for the bilayer is likely due to marked redistribution of electron density in the region between the outermost Ag layer and the underlying Mg^{2+}. This will be further discussed in section 3.3.

3.2. Density of States. In this study we have chosen to project the DOS onto the O 2p and Ag 4d basis functions because they should dominate the interfacial interaction. It is important to stress that we are not projecting the DOS onto any atomic orbital even though this is sometimes stated in the literature. Thus, what we refer to as O 2p includes all p functions in the 8−51 basis set and Ag 4d includes the first set of d functions in the 311-31 basis. In principle, the Ag 4d orbital could have some contributions from other d functions in the 311-31 basis. As a check, PDOS calculations were performed for the more diffuse d functions on Ag, as well as for Mg 2p and Mg 3p; these projections were all found to be very weak in intensity and we therefore conclude that these basis functions do not contribute to the interaction between the Ag overlayer and the MgO slab and that the Ag 4d and O 2p functions we have chosen give a good description of how the Ag 4d and O 2p orbitals interact in the different Ag/MgO interface systems. The PDOSs for Ag 4sp, 5sp and Ag 6sp were also checked but were also found to be very weak in intensity in the valence band.

By comparing the total and projected DOSs for the interface systems with the reference systems (isolated MgO slab and isolated Ag layer), we can study the way in which the metal/oxide interaction alters the electronic structure of the two parts of the system. Here we will also use the DOS curves to assist in selecting the most appropriate system description with respect to substrate thickness and one-sided vs two-sided adsorption.

3.2.1. Total DOS and Differences between the System Descriptions. The DOSs for the different interface descriptions (three- and five-layer MgO with one-side adsorption, and five- and seven-layer MgO with two-sided adsorption) are compared in Figure 2. All the total DOS curves display a small low-energy peak and a large high-energy region with several peaks. The total DOS curves also display downshifts compared to the isolated slab for both the one- and two-sided adsorption models; the downshift increases with increasing coverage. This is in agreement with the trend in adsorption energy seen in Table 1. When the coverage is increased, the intensity of the high-energy region is also shifted toward lower energy. The DOS for bilayer adsorption (calculated for one-sided adsorption on a three-layer MgO slab and two-sided adsorption on five-layer MgO slab) does not follow the trend with increasing downshift for increasing coverage. The Ag bilayer/MgO has a high-energy region, which lies higher in energy than that of the monolayer/MgO DOS, but also has a peak between the large high-energy region and the small low-energy peak.

The downshift in DOS gives an explanation for the increasing $E_{ads/surf}$ with increasing substrate thickness (Table 1). For these quite thin slabs, the valence states of all substrate atoms are downshifted with respect to the isolated MgO slab and because the downshifts are roughly similar for systems of different thickness within the same adsorption model (one- or two-sided adsorption), a change in substrate thickness will increase the number of states that are lowered in energy and therefore the larger system (thicker substrate or two- vs one-sided adsorption) should have the lower energy. However, this argument cannot explain the difference between the one- and two-sided adsorption models because the increase in size due to two-sided adsorption

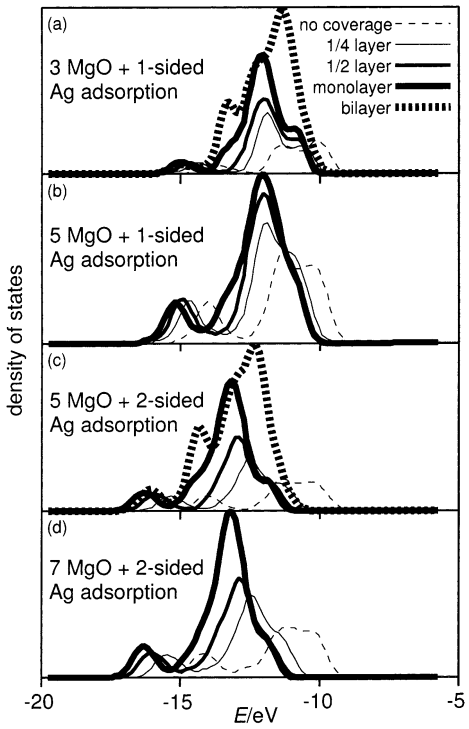

Figure 2. Total DOS (in the energy interval −20 to −5 eV corresponding to the upper valence band) for the four different Ag/MgO(001) models showing the effects of adsorption model (one- and two-sided adsorption), coverage, and substrate thickness. The maximum peak height has been normalized to the same value in all four sets of plots, but relative intensities within each of the four sets of plots are correct. Here and in all the following figures, the results are based on the Hartree−Fock electron density.

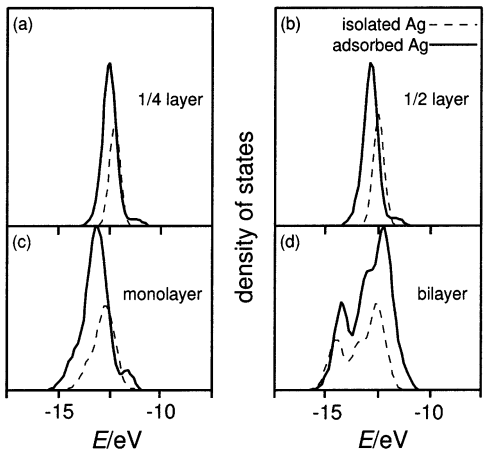

Figure 3. PDOS for Ag 4d for the adsorbed as well as the isolated Ag overlayers for all coverages. Here and in the following, all figures refer to two-sided adsorption on a 5-layer MgO slab. The difference in the areas under the isolated-Ag and adsorbed-Ag curves in each figure is due to the fact that there are twice the number of states under the adsorbed-Ag curves (2-sided adsorption).

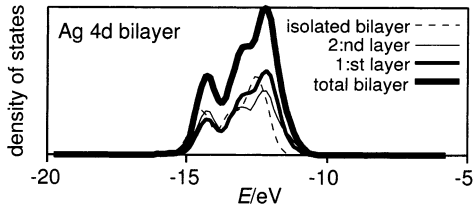

Figure 4. PDOS for the Ag 4d PDOS for the adsorbed bilayer separated for the first and second layer of Ag (the first layer being the layer closest to the substrate).

is compensated by a doubling of n_{surf} when $E_{ads/surf}$ is calculated (section 2.2).

It has been shown by Causà et al.[39] that already with a three-layer slab the electron density at the center of the slab is similar to the electron density of the bulk. Our calculation points to the same conclusion; in Figure 2 only slight changes in intensity can be seen when going from a three-layer to a five-layer substrate. However, when the one- and two-sided adsorption models for the five-layer substrate are compared, some differences can be seen (Figure 2). For two-sided adsorption the DOS downshift (with respect to the isolated MgO slab) is more pronounced than for one-sided adsorption. This is true for all coverages studied here and could be the reason for the difference in $E_{ads/surf}$ between the two adsorption models.

A possible explanation for the difference between the one- and two-sided adsorption is that there might be interactions between the *upper* and the *lower* Ag layers even though they are separated by five layers of MgO. For this reason a seven-layer slab with two-sided adsorption was studied. However, when the two-sided adsorption models for the five- and seven-layer substrates are compared, no significant differences for the DOSs could be found. It is therefore unlikely that there are significant interactions between the silver layers in the five-layer two-sided adsorption model either, because these would then surely decrease substantially when two extra layers of MgO were added to the substrate. Another more reasonable explanation for the differences in DOS between the one- and two-sided adsorption models could be the presence of a nonzero *z*-component of the dipole moment across the one-sided slab. This dipole moment might weaken the interfacial interaction. Despite the fact that a nonzero *z*-component of the dipole moment is indeed physical, it becomes energetically unfavorable because the slab is infinite. In nature such a dipole moment could perhaps occur locally, but not for the entire surface. An interface formed in reality would probably undergo structural rearrangements to prevent polarization of the entire surface. The two-sided adsorption model provides an easy way of canceling out the dipole moment. In summary, we conclude that the five-layer two-sided adsorption model gives a reasonable description of the system at a relatively low computational effort. The rest of the discussion will therefore focus on the results for this model.

3.2.2. Projected Density of States (PDOS). PDOS curves for Ag 4d for different overlayers of Ag on a five-layer thick MgO slab (two-sided adsorption) are compared with their isolated counterparts in Figure 3. For all coverages, except the bilayer, the Ag 4d PDOS is downshifted for the interface compared to the isolated Ag layer (Figure 3). Like for the total DOS, the downshift increases as the Ag coverage increases, but this trend is seen for the isolated Ag overlayers as well and is therefore not an effect of interfacial interactions (Figure 3). Nevertheless, the downshift for the Ag overlayers indicates further stabilization of the Ag layer for $\theta = {}^1/_4$, ${}^1/_2$ and 1.

The bilayer Ag 4d PDOS curve shows the same main features as the total DOS curve for the bilayer/MgO system. The bilayer/MgO system is similar to the curve for the isolated bilayer, but upshifted (Figure 3d). When the Ag 4d PDOS is projected onto the first and second layer atoms, respectively (the first layer being the layer closest to the substrate), one can see that the first-layer PDOS is slightly shifted to higher energies compared to the second-layer PDOS (Figure 4). This means that already for the second layer in an adsorbed bilayer, the electronic structure of Ag starts to resemble the corresponding layer in the isolated bilayer. The lack of downshift for the Ag 4d PDOS for the adsorbed bilayer seems contradictory to the trend in

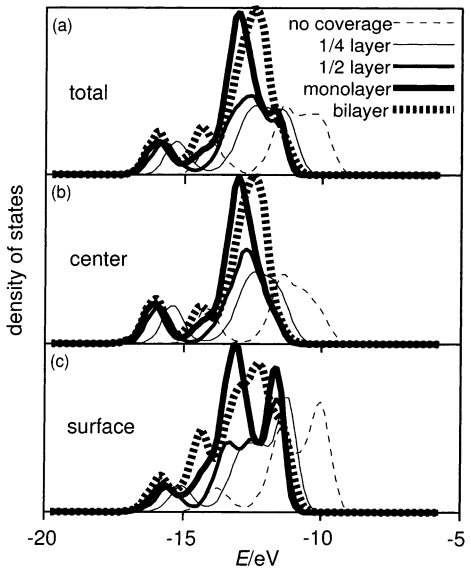

Figure 5. Total O 2p PDOS and projections onto the central and surface layer.

$E_{ads/surf}$ seen in section 3.1 and Table 1. However, as suggested in refs 23−25, the interfacial Ag/MgO bond is largely characterized by electrostatic interactions between the oxide and the redistributed electron density of the metal overlayer. The Ag 4d PDOS only describes the changes in the Ag overlayer and not the changes for the interface as a whole, which is seen in the total DOS (Figure 2).

Let us now turn to the O 2p PDOS (Figure 5). Here the trend of increasing downshift with increasing coverage is again seen, except for the bilayer adsorption, where the O 2p PDOS is slightly upshifted compared to the monolayer coverage. The downshifts are the same for the central layer of the substrate and the surface layers, but the shape of the surface layer O 2p PDOS is different from that of the middle region. This becomes even more obvious when the DOS is projected only onto the O 2p functions of the O^{2-} ions just underneath the adsorbed Ag atom (not shown here). The PDOS of the *x*- and *y*-components of O 2p look similar to the total O 2p, whereas the *z*-component shows a more distinct change with respect to coverage, although the main features are largely the same as for the total O 2p PDOS. From the results in Figure 5 we conclude that not only the surface layer is affected by the adsorbed Ag layer. However, the surface regions for the Ag/MgO systems show several new features in the O 2p PDOS compared to the isolated MgO slab, and such substantial changes do not occur in the central region of the slab.

The results from the O 2p PDOS calculations do not exhibit any metal-induced gap states; such states were found in previous FLAPW DFT studies of Ag/MgO[13] and Pd/MgO.[24] In fact, the shifts seen in our calculations are quite contrary to the Pd/MgO study,[24] which gave an upshift for the substrate DOS compared to the isolated MgO slab, and this upshift was reduced when going from the surface layer toward the center of the slab. The reason for the difference between Ag and Pd is probably that the Pd states lie much higher in energy than the MgO states. In our calculations, the Ag states are found at almost the same energy as the MgO states and our results agree quite well with shifts seen in the previous DFT study of a Ag monolayer on MgO,[13] where the substrate DOS was downshifted and this shift was seen both for the middle and surface layers.

3.3. Electronic Charge Density and Multipolar Expansion. A qualitative view of the charge redistribution of the Ag/MgO-(001) system is best provided by mapping the electronic charge density, $\rho(\vec{r})$, in cross sections perpendicular to the (001) surface. In each case, the sum of the total densities for the two components (the isolated MgO surface and the isolated Ag layer, both with the same geometry as in the total system) was subtracted from the $\rho(\vec{r})$ of the total system. Thus the resulting difference density maps, $\Delta\rho(\vec{r})$, display the charge redistribution caused by the interfacial interaction. This is the same type of $\Delta\rho(\vec{r})$ used in previous papers,[13,23,24] and we find such maps more illustrative than using a subtraction of atomic electron densities,[25,29,30] for cases when an interface is to be compared with its two isolated components. The $\rho(\vec{r})$ maps were complemented with multipolar expansions to provide a more quantitative description of the charge redistribution.

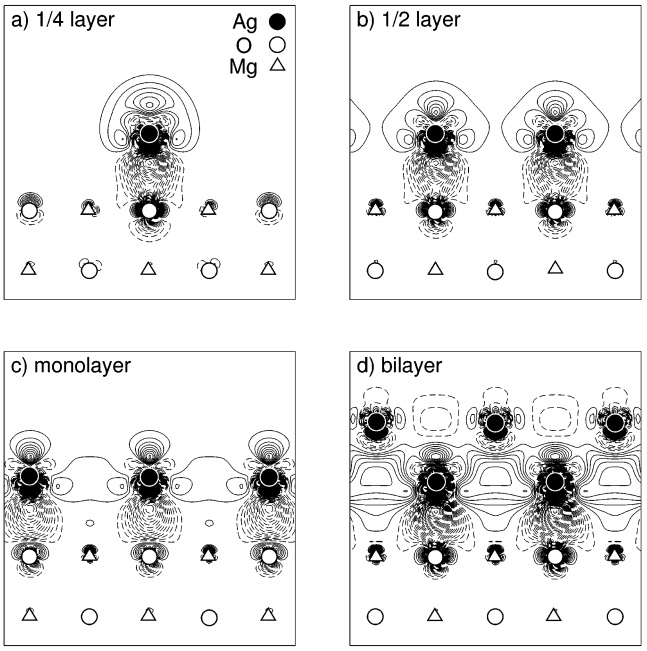

Figure 6. $\Delta\rho(\vec{r})$ for $^1/_4$, $^1/_2$, monolayer, and bilayer coverages. Solid lines indicate gain in electron density and dashed lines indicate loss. The zero contour level is omitted. The contour level interval is 0.0025 $e/Å^3$. All the indicated atoms lie in the plane of the paper.

The $\Delta\rho(\vec{r})$ maps for the $^1/_4$ Ag coverage (Figure 6a) clearly show how the Ag atom is polarized by the substrate and that the electron density is pushed away from the interfacial region. At $^1/_2$ Ag coverage (Figure 6b), a distortion of the Ag electron density has occurred as compared to the $^1/_4$ Ag coverage. Some electron density moves toward the vacant space above the Mg ion next to the adsorption site. This tendency becomes more pronounced for the Ag monolayer. As expected, for the Ag bilayer the electron density redistribution is more enhanced in the interfacial layer. For the Ag double layer also the topmost layer of Ag atoms contributes to the $\Delta\rho(\vec{r})$ in the space above the Mg^{2+} ion.

The changes in the substrate electron density on interfacial bonding is weaker than the changes that occur in the Ag overlayer. However, one can see that the Ag adsorption seems to reduce the electron density between the top layer O^{2-} and the Mg^{2+} ions just below them and that the electron density around the O^{2-} ions in the top layer is increased in the *xy*-plane.

The $\Delta\rho(\vec{r})$ maps display no noticeable differences between the one-sided adsorption and the two-sided adsorption models. This means that, for the contour level interval we have chosen, the $\rho(\vec{r})$ is not sensitive enough to display such tiny features or, differently put, the differences between the two models give

TABLE 2: Mulliken Charges on Ag (q_{Ag}) as Well as Projections of Dipole and Quadrupole Moments Normal to the Surface ($D_{Ag}^{(z)}$ and $Q_{Ag}^{(2z^2-x^2-y^2)}$, Respectively for the Ag/MgO(001) Interface for Various Substrate Coverages (θ) (Two-Sided Ag Adsorption on a Five-Layer MgO Slab)[a]

θ	q_{Ag}/e	$D_{Ag}^{(z)}/(e$ bohr)	$Q_{Ag}^{(2z^2-x^2-y^2)}/(e$ bohr$^2)$[b]
$^1/_4$	0.056	0.254 (0.000)	−0.427 (−0.039)
$^1/_2$	0.039	0.229 (0.000)	−1.429 (−1.213)
1	0.016	0.201 (0.000)	−1.993 (−1.549)
2	0.039[c]	0.405 (0.156)[c]	−1.466 (−0.385)[c]

[a] The values inside parentheses are for the isolated Ag slabs. [b] Negative values mean that the electron density is contracted along *z* and expanded in the interfacial *xy*-plane. [c] For the Ag layer closest to the substrate.

TABLE 3: Bond Population Analysis for the Ag−Ag and the Ag−O Interaction for the Ag/MgO(001) Interface (Two-Sided Ag Adsorption on a Five-Layer MgO Slab)[a]

θ	r_{Ag-Ag}/Å	p_{Ag-Ag}/e	r_{Ag-O}/Å	p_{Ag-O}/e[b]
$^1/_4$	5.742	0.000 (0.000)	2.61	−0.027
$^1/_2$	4.060	0.037 (0.035)	2.61	−0.025
	5.742	0.001 (0.001)		
1	2.871	0.107 (0.104)	2.70	−0.032
	4.060	0.021 (0.019)		
2, first layer[c]	2.871	0.083 (0.010)	2.51	−0.075
	4.060	0.013 (0.000)		
2, interlayer	2.871	0.065 (0.062)		
2, second layer[c]	4.060	0.007 (0.010)		

[a] The values in parentheses are for the isolated Ag slabs. [b] Values for the bond population between nonequivalent atoms must be multiplied by two when compared to standard molecular calculations.[33] [c] The first layer is the layer closest to the substrate. The two distances are the nearest and next-nearest distances, respectively; see Figure 1.

rise to features smaller than 0.0025 e/Å^3. A decreased contour level would reveal finer features but also make the $\Delta\rho(\vec{r})$ maps less readable.

The qualitative information concerning the electron density distribution caused by the interface formation can be further elucidated from a multipolar analysis (Table 2). Only a very small charge transfer takes place between the silver layer and the magnesia substrate: less than 0.05 e is transferred from the substrate to the adsorbate atoms. The value of atomic dipole moment projection, $D_{Ag}^{(z)}$, is larger for the $^1/_4$ coverage than for the monolayer coverage (see Table 2). At the same time, the quadrupole moment projection $Q^{(2z^2-x^2-y^2)}$ for the $^1/_4$ coverage is significantly smaller than that for the silver monolayer (Table 2).

The bond population analysis (Table 3) supports our conclusions for the other electronic properties. The Ag−Ag overlap population is slightly increased for all interfaces compared to the isolated systems. For the Ag bilayer, a short-range (2.87 Å) overlap within the first layer is only present in the adsorbed Ag bilayer, whereas such overlaps do occur between the first and second Ag layers in both the adsorbed and isolated Ag bilayers. These results show that there is an attractive interaction between the Ag−Ag overlap density and the Mg^{2+} ion in the substrate below; this enhances as well as distorts the Ag−Ag overlap. These bond population results confirm what was indicated in the $\Delta\rho(\vec{r})$ maps. There also exists a small (0.001−0.002 e) overlap population between Ag and Mg^{2+}.

The overlap between Ag and O^{2-} is fairly constant for coverages up to $\theta = 1$ and shows the antibonding character of the interaction. For the bilayer, the overlap population is also antibonding, but twice as large as for the other systems. This agrees with the results from the DOS analysis where an upshift in DOS was seen for the bilayer adsorption compared to the other interfaces.

4. Conclusions

Our ab initio calculations show that for all interface models used in this study, the DOS is downshifted when the substrate coverage is increased. For both one- and two-sided adsorption, the downshift of the O 2p PDOS suggests a stabilization of the substrate due to the interaction between the 2p and 4d orbitals on O and Ag, respectively. Also, the Ag layers seem to be more stabilized in the two-sided adsorption model than in the one-sided adsorption model. In general, we see that the two-sided adsorption model gives slightly larger downshifts and thus stabilizes the system slightly more than the one-sided adsorption model. For two-sided adsorption, also the trend of an increased downshift with increased Ag coverage is more pronounced. These differences are most likely caused by a nonzero *z*-component of the dipole moment perpendicular to the slab in the one-sided case.

The difference electron density confirms results from previous studies[16,23,25] with significant charge redistribution in the Ag overlayer, mainly involving a polarization of the Ag electron density in the *z*-direction for low θ, but enhanced electron density in the *xy*-plane is also seen as the θ increases. The presence of the substrate enhances the delocalization of the Ag electron density compared to the free Ag layer. These charge redistributions are confirmed by the multipolar expansion analysis, where the $D_{Ag}^{(z)}$ and $Q^{(2z^2-x^2-y^2)}$ values are enhanced for low and high coverages, respectively. The bond population analysis shows the Ag−Ag overlap population to be higher for the adsorbed Ag overlayers compared to the isolated Ag slabs.

We can also see from our results that, whereas the monolayer and submonolayer coverages follow a quite regular trend in the changes of the electronic properties with increasing coverage, the bilayer adsorption behaves rather differently. The electronic properties studied in this paper show that for $^1/_4$, $^1/_2$, and 1 monolayer coverages, the overlap density in the Ag overlayer is localized in the *xy*-plane. For the isolated bilayer, the bond population shows that the overlap occurs mainly between the two Ag layers and not within each layer. Thus the overlap occurs in the *z*-direction instead of the *xy*-plane. The bond population and quadrupole moments show that the overlap density increases in the *z*-direction and decreases in the *xy*-plane when θ is increased from 1 to 2. This can explain the different behavior of the adsorbed bilayer.

From this study we conclude that the interfacial interaction arises from a charge redistribution within both components of the interface (the MgO substrate and the Ag overlayer), although the redistribution is more pronounced in the Ag overlayer. This can be seen in the $\Delta\rho(\vec{r})$ and the Ag−Ag bond population. The redistribution leads to electrostatic interactions between the polarized Ag atoms and O^{2-} ions and between the enhanced $\rho(\vec{r})$ between the Ag atoms and Mg^{2+} ion. We believe that the electrostatic potential created by the polarized Ag layer is the explanation for the downshifts in DOS for all adsorption models we have studied. The DOS curves also reveal that some overlap between O 2p and Ag 4d states exist, but the Mulliken charges suggest that charge transfer across the interface is negligible and the bond population shows that the Ag−O^{2-} overlap is mainly antibonding, especially for bilayer adsorption.

Acknowledgment. This study was supported by the Swedish Foundation for International Cooperation in Research and Education (STINT), the Swedish Research Council (VR), the

Royal Swedish Academy of Sciences (KVA) and the European Center of Excellence for Advanced Materials Research and Technology (contract No. ICA1-CT-2000-7007), Riga.

References and Notes

(1) Henrich, V. E.; Cox, P. A. *The Surface Science of Metal Oxides*; University Press: Cambridge, U.K., 1993.
(2) Finnis, M. W. *J. Phys.: Condens. Matter* **1996**, *8*, 5811.
(3) Noguera, C. *Physics and Chemistry at Oxide Surfaces*; University Press: Cambridge, U.K., 1996.
(4) Campbell, C. T. *Surf. Sci. Rep.* **1997**, *27*, 1.
(5) Trampert, A.; Ernst, F.; Flynn, C. P.; Fishmeister, H. F.; Rühle, M. *Acta Metall. Mater.* **1992**, *40*, 227.
(6) Didier, F.; Jupille, J. *Surf. Sci.* **1994**, *307*−*309*, 587.
(7) Schaffner, M.-H.; Patthey, F.; Schneider, W.-D. *Surf. Sci.* **1998**, *417*, 159.
(8) Robach, O.; Renaud, G.; Barbier, A. *Phys. Rev. B* **1999**, *60*, 5858.
(9) Suzuki, T.; Hishita, S.; Oyoshi, K.; Souda, R. *Surf. Sci.* **1999**, *442*, 291.
(10) Larsen, J. H.; Ranney, J. T.; Starr, D. E.; Musgrove, J. E.; Campbell, C. T. *Phys. Rev. B* **2001**, *63*, 195410.
(11) Stracke, P.; Krischok, S.; Kempter, V. *Surf. Sci.* **2000**, *473*, 86.
(12) Schönberger, U.; Andersen, O. K.; Methfessel, M. *Acta Metall. Mater.* **1992**, *40*, 1.
(13) Li, C.; Wu, R.; Freeman, A. J.; Fu, C. L. *Phys. Rev. B* **1993**, *48*, 8317.
(14) Purton, J. A.; Bird, D. M.; Parker, S. C.; Bullett, D. W. *J. Chem. Phys.* **1999**, *110*, 8090.
(15) Cho, J.; Kim, K. S.; Chan, C. T.; Zhang, Z. *Phys. Rev. B* **2001**, *63*, 113408.
(16) Hong, T.; Smith, J. R.; Srolovitz, D. J. *J. Adhesion Sci. Technol.* **1994**, *8*, 837.
(17) Duffy, D. M.; Harding, J. H.; Stoneham, A. M. *Acta Metall. Mater.* **1995**, *43*, 1559.
(18) Ferrari A. M.; Pacchioni G. *J. Phys. Chem.* **1996**, *100*, 9032.
(19) Benedek, R.; Minkoff, M.; Yang, L. H. *Phys. Rev. B* **1996**, *54*, 7697.
(20) Yudanov, I. V.; Vent, S.; Neyman, K. M.; Pacchioni, G.; Rösch, N. *Chem. Phys. Lett.* **1997**, *275*, 245.
(21) Purton, J.; Parker, S. C.; Bullett, D. W. *J. Phys.: Condens. Matter* **1997**, *9*, 5709.
(22) Stoneham, A. M.; Harding, J. H. *Acta Metall. Mater.* **1998**, *46*, 11155.
(23) Heifets, E.; Zhukovskii, Yu. F.; Kotomin, E. A.; Causà, M. *Chem. Phys. Lett.* **1998**, *283*, 395.
(24) Goniakowski, J. *Phys. Rev. B* **1998** *57*, 1935; **1998**, *58*, 1189.
(25) Zhukovskii, Yu. F.; Alfredsson, M.; Hermansson, K.; Heifets, E.; Kotomin, E. A. *Nucl. Instrum. Methods Phys. Res. B* **1998**, *141*, 73.
(26) Lopez, N.; Illas, F.; Rösch, N.; Pacchioni, G. *J. Chem. Phys.* **1999**, *110*, 4873.
(27) Matveev, A. V.; Neyman, K. M.; Yudanov, I. V.; Rösch, N. *Surf. Sci.* **1999**, *426*, 123.
(28) Musolino, V.; Selloni, A.; Car, R. *Phys. Rev. Lett.* **1999**, *83*, 3242.
(29) Zhukovskii, Yu. F.; Kotomin, E. A.; Jacobs, P. W. M.; Stoneham, A. M.; Harding, J. H. *Surf. Sci.* **1999**, *441*, 373.
(30) Zhukovskii, Yu. F.; Kotomin, E. A.; Jacobs, P. W. M.; Stoneham, A. M.; Harding, J. H. *J. Phys.: Condens. Matter* **2000**, *12*, 55. Zhukovskii, Yu. F.; Kotomin, E. A.; Jacobs, P. W. M.; Stoneham, A. M. *Phys. Rev. Lett.* **2000** *84*, 1256.
(31) Kantorovich, L. N.; Shluger, A. L.; Sushko, P. V.; Günster, J.; Stracke, P.; Goodman, D. W.; Kempter, V. *Faraday Discuss.* **1999**, *114*, 173.
(32) Fuks, D.; Dorfman, S.; Kotomin, E. A.; Zhukovskii, Yu. F.; Stoneham, A. M. *Phys. Rev. Lett.* **2000**, *85*, 4333.
(33) Saunders, V. R.; Dovesi, R.; Roetti, C.; Causà, M.; Harrison, N. H.; Orlando, R.; Zicovich-Wilson, C. M. *CRYSTAL98 Users Manual*; University Torino: Turin, Italy, 1999.
(34) Dowben, P. A. *Surf. Sci. Rep.* **2000**, *40*, 151.
(35) Perdew J. P.; Wang, Y. *Phys. Rev. B* **1992**, *45*, 13244.
(36) Lee, C.; Yang, W.; Parr, R. G. *Phys. Rev. B* **1988**, *37*, 785.
(37) Perdew, J. P.; Zunger, A. *Phys. Rev. B* **1981**, *23*, 5048.
(38) Vosko, S. H.; Wilk, L.; Nusair, M. *Can. J. Phys.* **1980**, *58*, 1200.
(39) Causà, M.; Dovesi, R.; Pisani, C.; Roetti, C. *Surf. Sci.* **1986**, *175*, 551.
(40) Hay, P. J.; Wadt, W. R. *J. Chem. Phys.* **1985**, *82*, 284.
(41) Aprà, E.; Stefanovich, E. V.; Dovesi, R.; Roetti, C. *Chem. Phys. Lett.* **1991**, *186*, 329
(42) Guest, M. F.; Saunders, V. R. *Mol. Phys.* **1974**, *28*, 819.
(43) Pisani, C.; Dovesi R.; Roetti, C. *Lecture Notes in Chemistry, vol. 48 Hartree*−*Fock Ab initio Treatment of Crystalline Systems*; Springer: Berlin, 1988.